Available online at www.sciencedirect.com
ScienceDirect
Polymer 48 (2007) 6325–6339
polymer
www.elsevier.com/locate/polymer

Morphology and properties of nanocomposites formed from ethylene-vinyl acetate copolymers and organoclays

Lili Cui [a], Xiaoyan Ma [a,b], D.R. Paul [a,*]

[a] Department of Chemical Engineering, The University of Texas at Austin, Austin, TX 78712, USA
[b] Department of Applied Chemistry, School of Science, Northwestern Polytechnical University, Xi'an, Shaanxi 710072, PR China

Received 20 June 2007; accepted 14 August 2007
Available online 22 August 2007

Abstract

A series of ethylene-vinyl acetate copolymers, EVA, containing 0–40% VA and three organoclays, $M_2(HT)_2$, $M_3(HT)_1$ and $(HE)_2M_1T_1$, were melt processed to explore the relationship between the polarity of the polymer matrix and the organoclay structure on the extent of exfoliation and properties of the resulting nanocomposites. The degree of exfoliation of the nanocomposites was evaluated by TEM, WAXS, and mechanical testing. Quantitative particle analyses of TEM images were made to give various averages of the clay dimensions and aspect ratio. The results from different techniques were generally consistent with each other. These EVA copolymer nanocomposites show dramatically improved exfoliation of the organoclay as the VA content is increased. Nanocomposites based on the organoclay with two alkyl tails always gave better exfoliation than those based on the organoclays with a single tail at all VA levels; however, the relative advantage of the two tails versus one tail seems to diminish with increased VA level. The predictions of tensile modulus using a simple composite model based on Halpin–Tsai equations show rather good agreement with the experimental data.

Keywords: Ethylene-vinyl acetate copolymers; Nanocomposites; Organoclays

1. Introduction

Polymer nanocomposites prepared from high aspect ratio platelets of clays like montmorillonite may achieve significant improvements in mechanical, thermal, barrier, and flammability properties at very low filler concentrations [1–3], compared to conventional composites, without a significant increase in density or loss of optical properties. To take advantage of the high aspect ratio of these silicate platelets, the challenge is to exfoliate the individual platelets within the polymer matrix which requires favorable polymer–organoclay interactions.

Ammonium surfactants are usually used to modify montmorillonite clay to gain better affinity between the hydrophilic aluminosilicate clay and the organophilic polymer matrix; polymers with different levels or types of polarity may require different surfactant structures to achieve the best exfoliated structure. Previous studies in our laboratory showed that nylon 6-based nanocomposites have the best exfoliation when the organoclay is formed from a surfactant with only one long alkyl tail [4,5]; on the other hand, polyolefin matrices give better exfoliation with organoclays modified by a surfactant with two or more long alkyl tails [6–9].

Ethylene-vinyl acetate (EVA) copolymers are a class of widely used polymers, with a variety of industrial applications such as cable and wire, flexible packaging, hose and tube, photovoltaic encapsulants and footwear. They contain polar vinyl acetate and non-polar ethylene units in the polymer chain. By varying the vinyl acetate content, EVA copolymers can be tailored for applications as rubbers, thermoplastic elastomers and plastics. Recently there has been interest in improving the flammability characteristics of EVA copolymers, for their application in wire and cable jackets and insulation, by melt blending with organoclays [10–14].

* Corresponding author. Tel.: +1 512 471 5392; fax: +1 512 471 0542.
E-mail address: drp@che.utexas.edu (D.R. Paul).

0032-3861/$ - see front matter © 2007 Elsevier Ltd. All rights reserved.
doi:10.1016/j.polymer.2007.08.040

This paper explores the relationship between the polarity of the polymer matrix and the organoclay structure on the extent of exfoliation and properties of the resulting nanocomposites. Our rationale for choosing ethylene-vinyl acetate copolymers as the matrix is as follows. By adjusting the VA concentration in the EVA copolymer, the polymer–organoclay interactions can be varied. In doing so, the optimum surfactant structure may switch from the type that works best for polyolefins (two or more tails) to that works best for very polar polymers like nylon 6 (one tail) as the VA content is increased.

2. Experimental

2.1. Materials

Table 1 describes the commercially available grades of ethylene-vinyl acetate copolymers supplied by DuPont and a comparable grade of LDPE from Novapol used in this work. These polymers have a similar melt index of 2–3 g/10 min, with vinyl acetate contents ranging from 0 to 40 wt%.

Organoclays, generously donated by Southern Clay Products, Inc., were formed by cation exchange between sodium montmorillonite (CEC = 92 meq/100 g clay) and various quaternary ammonium salts. Some frequently used abbreviations are employed here to represent the substituents on the ammonium cation, e.g., M for methyl and HE for 2-hydroxy-ethyl, while T and HT represent long alkyl chains from natural tallow oil and hydrogenated tallow, respectively. These organoclays were selected to explore the effects of the ammonium surfactant structure on the dispersion of the clay particles in different EVA copolymer matrices. $M_2(HT)_2$ and $M_3(HT)_1$ organoclays allow a comparison of the effect of a number of long alkyl tails, while the $M_3(HT)_1$ and $(HE)_2M_1T_1$ organoclays allow a comparison of the effect of having hydroxyl functional groups versus not having any (Table 2).

Table 1
Polymers used in this study

Materials	Trade name	Supplier	wt% VA	MI (g/10 min)	Density (g/cm^3)	Melting temperature (°C)
LDPE	LF-0219-A	Novapol	0	2.3	0.918	107
EVA-9.3	Elvax® 760Q	DuPont	9.3	2.0	0.93	100
EVA-18	Elvax® 460	DuPont	18	2.5	0.941	88
EVA-28	Elvax® 265	DuPont	28	3.0	0.951	73
EVA-40	Elvax® 40L-03	DuPont	40	3.0	0.966	58

Note: all the data shown in this table were obtained from the manufacturers.

2.2. Processing

EVA nanocomposites were prepared by melt compounding in a Haake, co-rotating, intermeshing twin screw extruder ($D = 30$ mm, $L/D = 10$) at a screw speed of 280 rpm with a feed rate of 1000 g/h, using a barrel temperature of 170 °C. EVA materials were dried in a vacuum oven for a minimum of 24 h prior to the compounding, while the organoclays were used as received.

For nanocomposites formed from LDPE, EVA-9.3, EVA-18 and EVA-28, tensile (ASTM D638) and Izod (ASTM D256) specimens were formed using an Arburg Allrounder 305-210-700 injection molding machine. Due to the difficulty of injection molding EVA-40, a DSM Micro 5 melt compounder was used to melt the nanocomposites formed with the twin screw extruder, and then a DSM micro-injection molding machine was used to make small rectangular bars ($0.32 \times 1.00 \times 7.10$ cm). Both injection molding operations were conducted at a barrel temperature of 180 °C and a mold temperature of 25 °C, with injection pressure and holding pressure both set at 40 bar. After molding, the specimens were immediately sealed in a polyethylene bag and placed in a vacuum desiccator for a minimum of 24 h prior to mechanical testing. For EVA-40 based nanocomposites, mechanical testing was not performed; however, the morphology was examined by TEM and WAXS.

The data below are reported in terms of the weight percent montmorillonite (MMT) in the composites rather than the amount of organoclay, since the silicate is the reinforcing component. The amount of montmorillonite in the nanocomposite was determined by placing pre-dried nanocomposite pellets in a furnace at 900 °C for 45 min and weighing the remaining MMT ash. A correction for loss of structural water was made in the calculation [15–17].

2.3. Characterization

TEM images were obtained using a JEOL 2010F transmission electron microscope operating under an accelerating voltage of 120 kV. Ultra-thin sections (~50 nm) were cut from the central part of the rectangular injection molded bars in the plane parallel to the flow direction under cryogenic conditions using an RMC PowerTome XL microtome.

X-ray diffraction scans were obtained using a Scintag XDS 2000 diffractometer in the reflection mode, using an incident X-ray wavelength of 1.541 Å at a scan rate of 1.0 deg/min over the range of $2\theta = 1–12°$. The skin of the major faces

Table 2
Organoclays used in this study

Organoclay designation	SCP designation	Surfactant chemical structure	Specifications
$M_2(HT)_2$	Cloisite 20A	Dimethylbis(hydrogenated-tallow) ammonium montmorillonite	95 MER, $d_{001} = 2.42$ nm
$M_3(HT)_1$	SCPX 1137	Trimethyl hydrogenated-tallow ammonium montmorillonite	95 MER, $d_{001} = 1.80$ nm
$(HE)_2M_1T_1$	Cloisite 30B	Bis(2-hydroxy-ethyl)methyl tallow ammonium montmorillonite	90 MER, $d_{001} = 1.79$ nm

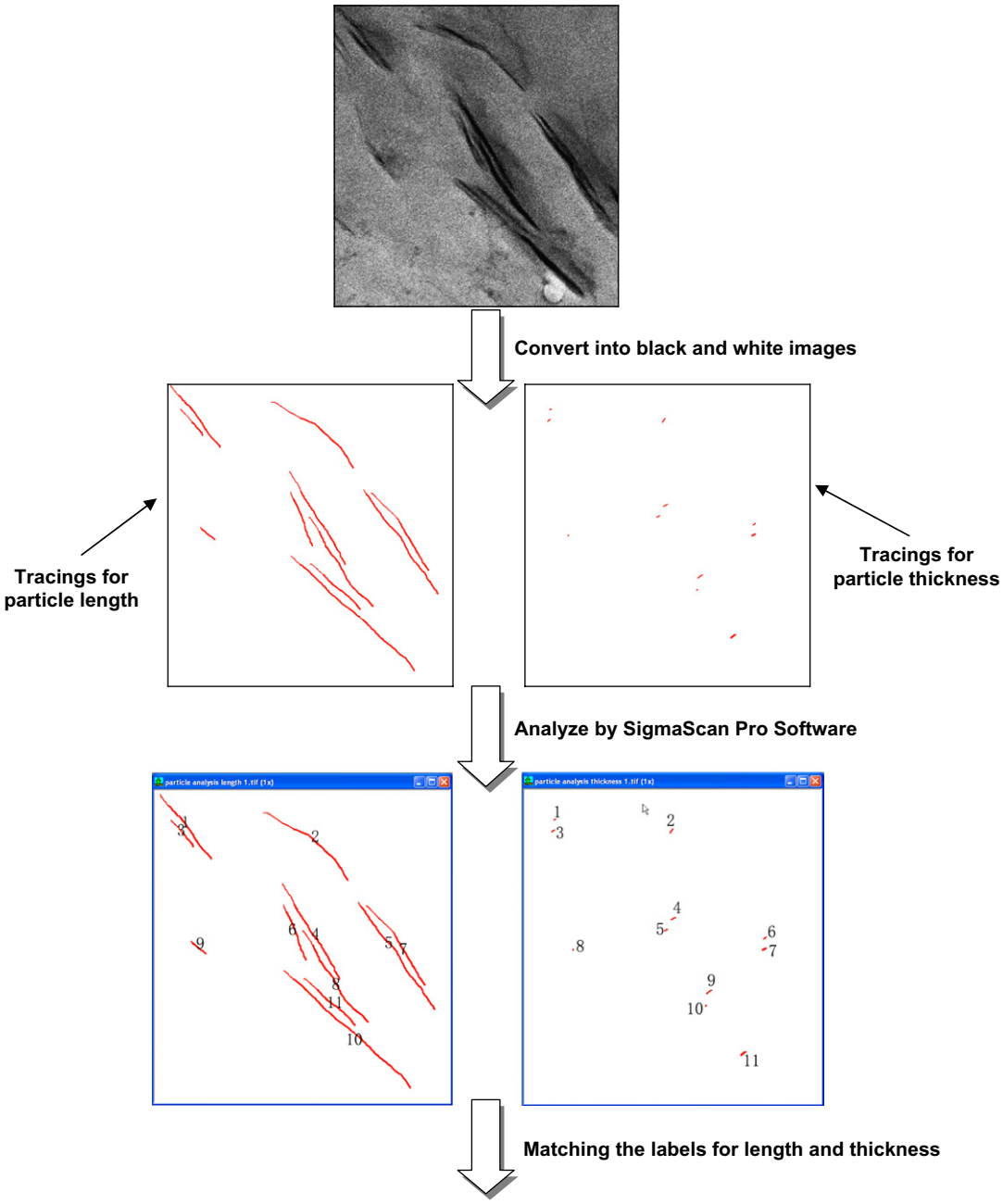

Length Labels	1	2	3	4	5	6	7	8	9	10	11
Thickness labels	1	2	3	4	7	5	6	9	8	11	10

Fig. 1. Illustration of particle analysis procedures.

of the injection molded rectangular bars was scanned while the organoclays were analyzed in powder form.

Tensile tests were performed on an Instron model 1137 machine upgraded for computerized data acquisition. Modulus values were determined using an extensometer at a crosshead speed of 0.51 cm/min. Elongation at break was measured at a crosshead speed of 5.1 cm/min. Data reported here represent an average from measurements on at least five specimens.

2.4. Particle analysis

An analysis of the clay particles was conducted using TEM images at a 10–15k magnification for each sample. Due to the low contrast of the TEM images, digital image files were saved in .tiff or .jpg format, which could be opened in Adobe Photoshop, where the dimensions of the dispersed platelets and agglomerates were traced into overlapped transparent layers. Two separate tracings were done for each TEM images,

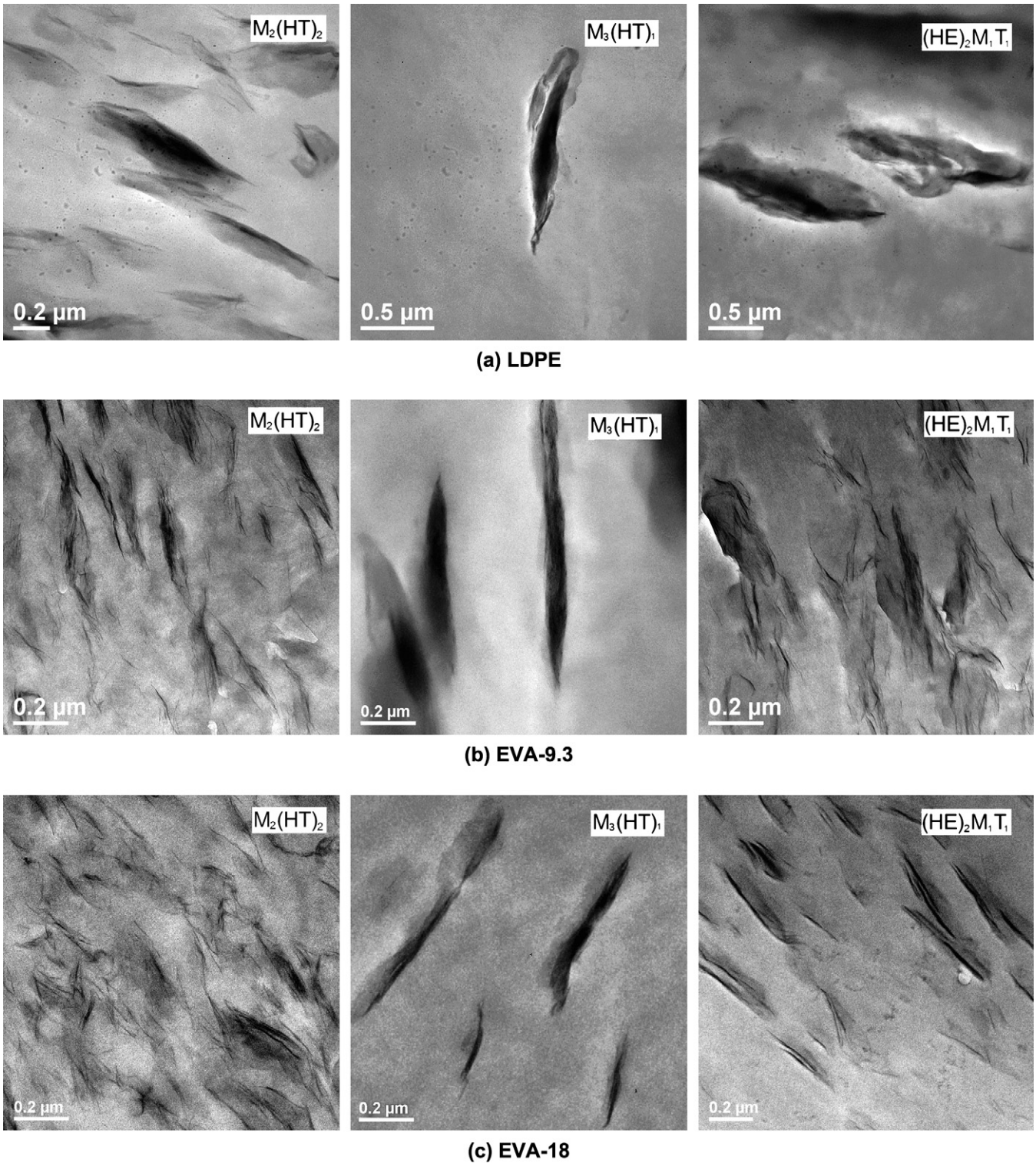

Fig. 2. TEM micrographs of nanocomposites containing ~5 wt% MMT based on different organoclays and prepared from various EVA copolymers (a) LDPE, (b) EVA-9.3, (c) EVA-18, (d) EVA-28 and (e) EVA-40.

one to measure the lengths of the particles and the other to measure particle thickness. For some nanocomposites with well-exfoliated structures, no attempt was made to measure the thickness of single platelets as this introduces relatively large errors; these particles were assigned to a thickness of 0.94 nm [18] corresponding to the known results for MMT platelets. The two resulting layers can be transferred to separate image files with high contrast for accurate analysis by SigmaScan Pro, the software used to analyze the traced particles in terms of both length and thickness. After analysis, two series of numbers were assigned to the length tracings and thickness tracings, respectively, and their characteristic dimensions

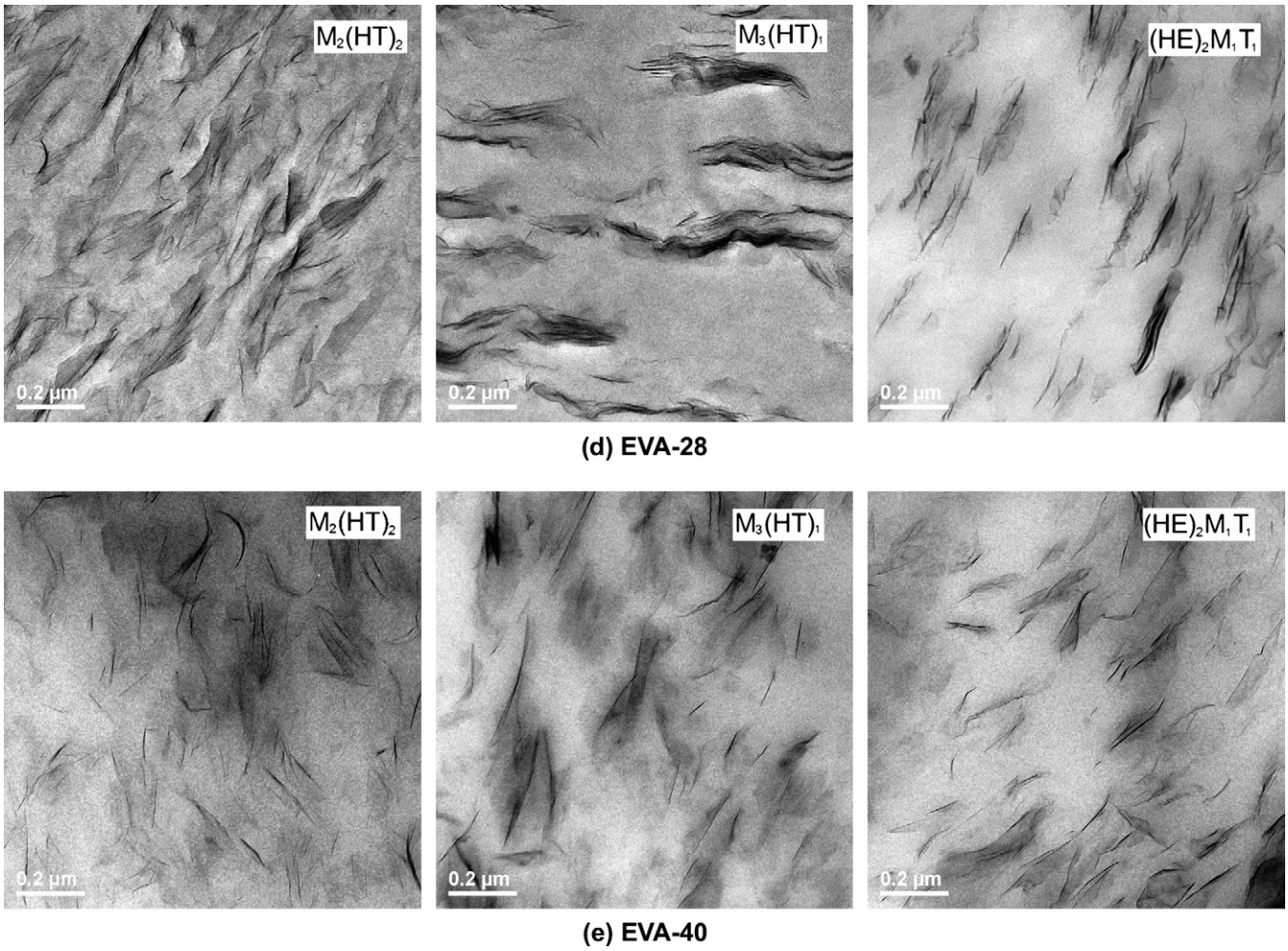

Fig. 2. (*Continued*)

were exported into two separate files. In this paper, four kinds of aspect ratios are reported, i.e., the number and weight averages of the aspect ratios determined for individual particles ($\langle l/t\rangle_n$ and $\langle l/t\rangle_w$) and ratios of the number or weight averages of particle lengths and thicknesses ($\bar{l}_n/\bar{t}_n$ and $\bar{l}_w/\bar{t}_w$). Since the measurement of the lengths and thicknesses of the

Table 3
Results of particle analysis of nanocomposites containing 5 wt% MMT

Organoclay	Vinyl acetate (wt%)	Total number of particles	Number average particle length ($\bar{l}_n$, nm)	Number average particle thickness ($\bar{t}_n$, nm)	Weight average particle length ($\bar{l}_w$, nm)	Weight average particle thickness ($\bar{t}_w$, nm)	Number average aspect ratio $\langle l/t\rangle_n$	$\bar{l}_n/\bar{t}_n$	Weight average aspect ratio $\langle l/t\rangle_w$	$\bar{l}_w/\bar{t}_w$
$M_2(HT)_2$	0	389	260	25.7	389	67.1	16.8	10.1	33.1	5.8
	9.3	265	243	13.1	301	20.8	26.5	18.5	37.7	14.5
	18	563	127	6.0	171	10.9	31.5	21.1	43.4	15.7
	28	611	130	5.9	182	12.6	39.0	21.9	69.1	14.5
	40	731	103	3.4	143	6.8	58.0	30.2	100.4	21.0
$M_3(HT)_1$	0	39	853	128.3	1419	258.9	9.1	6.6	15.1	5.5
	9.3	28	427	53.3	691	82.6	10.1	8.0	12.3	8.4
	18	167	402	57.5	574	101.0	9.4	7.0	14.1	5.7
	28	224	159	11.7	244	23.6	20.4	13.6	45.5	10.3
	40	605	117	4.4	164	7.7	49.9	26.8	101.5	21.2
$(HE)_2M_1T_1$	0	20	922	178.0	1112	265.2	7.5	5.2	10.2	4.2
	9.3	477	171	13.3	220	20.4	16.2	12.9	24.8	10.8
	18	495	216	13.1	299	28.3	20.6	16.5	28.6	10.6
	28	723	124	6.9	185	13.4	24.0	18.0	43.3	13.8
	40	791	107	3.4	148	6.5	56.6	31.2	105.6	22.9

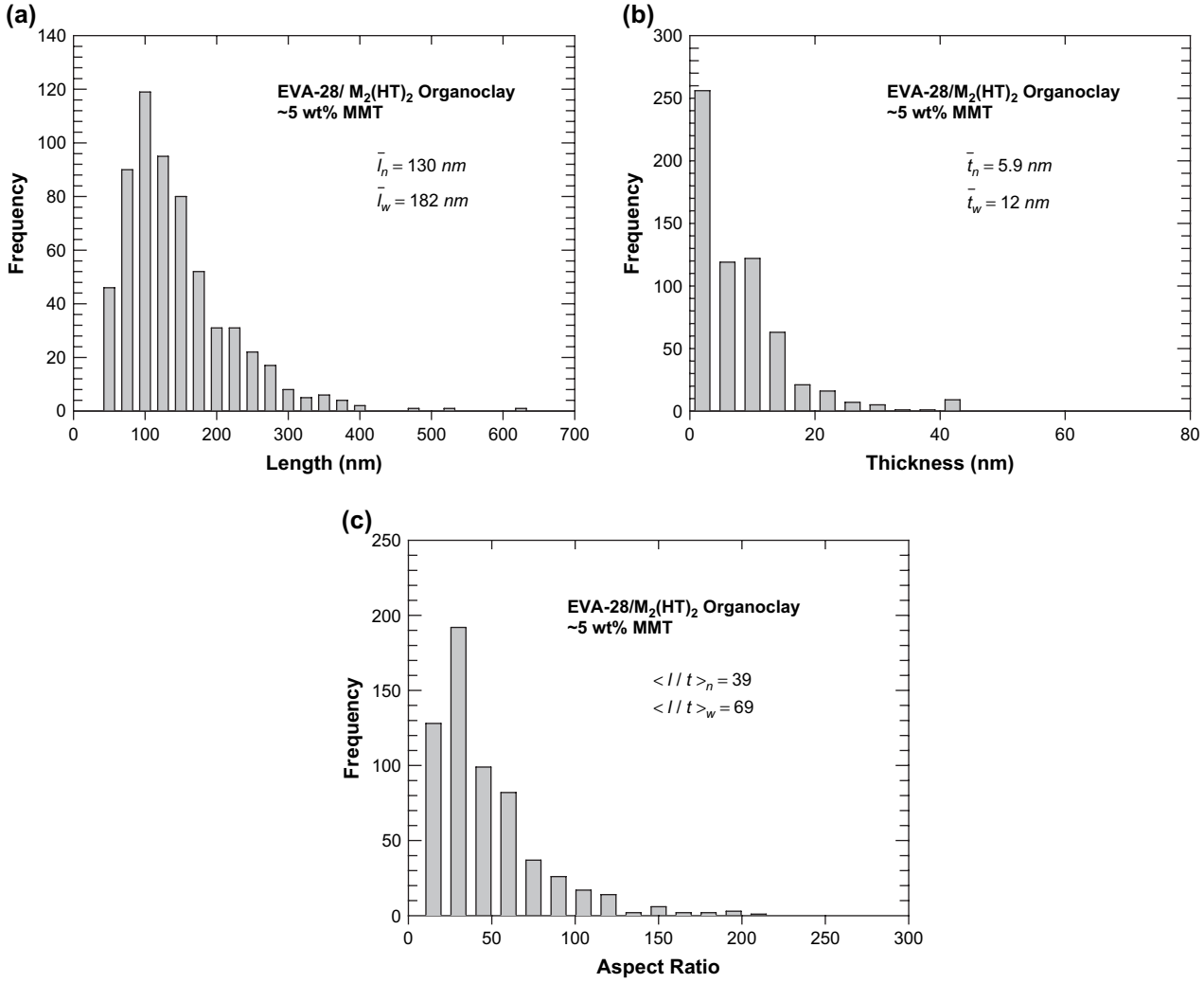

Fig. 3. Histograms of (a) particle length, (b) particle thickness, and (c) aspect ratio for EVA-28/$M_2(HT)_2$ nanocomposites with nominally 5 wt% MMT (total number of particles = 611).

particles was performed on different tracings, each particle is assigned two different numerical labels. To obtain the aspect ratio of individual particles, a manual matching of particles on the tracing for length must be made with particles on the tracing for thickness, and then from this file the number and weight averages, $\langle l/t \rangle_n$ and $\langle l/t \rangle_w$, can be calculated. The procedures for particle analysis are illustrated in Fig. 1.

3. Results and discussion

3.1. Morphology

3.1.1. Transmission electron microscopy

Properly prepared TEM images provide the most direct visualization of the dispersion of the clay particles in nanocomposites. Fig. 2 compares the morphology of nanocomposites based on polymer matrices containing from 0 to 40% VA formed from $M_2(HT)_2$, $M_3(HT)_1$, and $(HE)_2M_1T_1$ organoclays. The montmorillonite content in all cases is nominally 5 wt%.

When there are no polar groups in the polymer matrix, i.e., LDPE, the dispersion of the clay is poor and large tactoids can be seen in composites formed from all three kinds of organoclays, see Fig. 2(a). For the LDPE composites based on one-tailed organoclays, $M_3(HT)_1$ and $(HE)_2M_1T_1$, clay particles as large as 1 μm can be seen. For the LDPE/$M_2(HT)_2$ organoclay composites, the dispersion of clay particles is much better than that formed from the other two organoclays, and a mixture of small particles and larger agglomerates can be observed. These results are consistent with prior reports from this laboratory [9,19,20], i.e., non-polar polymers like polypropylene and polyethylene give nanocomposites with much better dispersion in the case of multiple tailed organoclays. Polyolefins are relatively compatible with alkyl tails and increasing the number of tails better shields the polar silicate surface from the polymer matrix as explained previously [9,19,20].

The presence of only 9.3 wt% VA units in the polymer matrix (see Fig. 2(b)) leads to significant improvement in exfoliation of the organoclay, particularly for $M_2(HT)_2$ or $(HE)_2M_1T_1$, compared to the corresponding LDPE-based

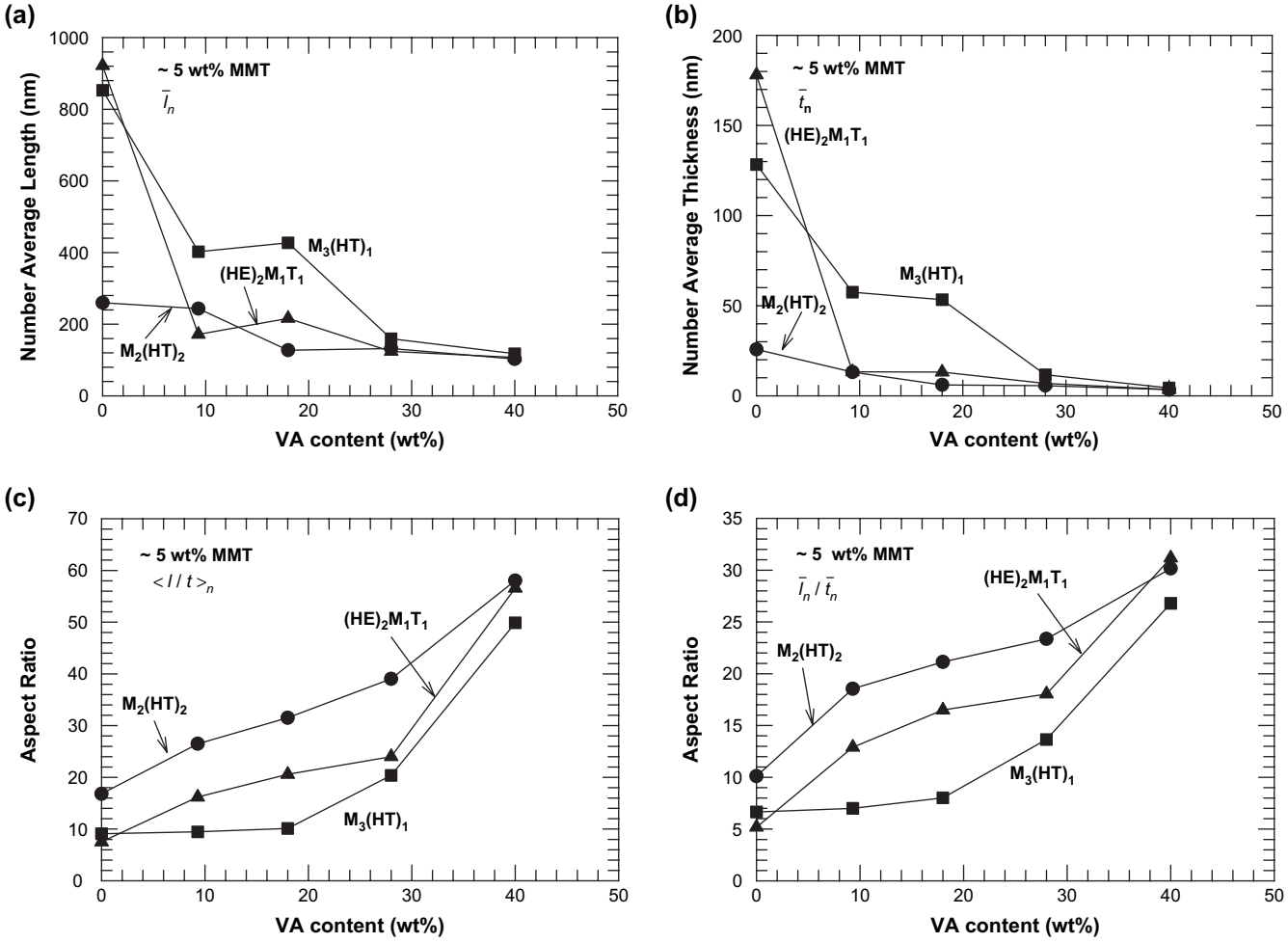

Fig. 4. The effect of vinyl acetate content on (a) particle length, (b) particle thickness, (c) number average aspect ratio, and (d) ratio of number average particle length and number average particle thickness of EVA nanocomposites at a fixed MMT content of ~5 wt%.

composites. Although clay tactoids are still observed, the particle size is reduced dramatically. The composite formed from the $M_3(HT)_1$ organoclay still produces the lowest number of particles with the largest size, and the dispersion of the clay particles changed only slightly compared to the LDPE-based composites. Clearly, the nanocomposite based on the $M_2(HT)_2$ organoclay still has the best exfoliation; thus, while addition of this level of VA has improved the polymer–organoclay interaction, this EVA still behaves more like a polyolefin than a polyamide with regard to the optimum number of tails for exfoliation. The potential for interactions between the hydroxyl groups of the surfactant and the acetate groups of the polymer adds a new consideration for nanocomposites formed from the $(HE)_2M_1T_1$ organoclay compared to that formed from the $M_3(HT)_1$ organoclay; note that it has also been argued that these hydroxyl groups in the $(HE)_2M_1T_1$ surfactant may be attracted to the clay surface [4,8,21,22] thereby shielding the polymer–silicate interactions.

TEM images of nanocomposites based on EVA-18 and EVA-28 are shown in Fig. 2(c) and (d). This further increase in VA content of the polymer matrix leads to continued improvement in exfoliation of the nanocomposites formed from each organoclay; again, the best exfoliation is seen in nanocomposites formed from the $M_2(HT)_2$ organoclay, with the $(HE)_2M_1T_1$ organoclay being next best, and the poorest exfoliation is seen for the nanocomposites formed from the $M_3(HT)_1$ organoclay.

Fig. 2(e) shows images for nanocomposites based on EVA-40; here, all the nanocomposites have a well-exfoliated morphology consisting predominantly of individual platelets dispersed uniformly throughout the polymer matrix. The nanocomposite formed from $M_3(HT)_1$ also exhibits highly exfoliated structures; however, upon close examination, the platelet delamination is slightly less complete than seen for the other two organoclays. On going from 28 to 40% VA in the matrix, nanocomposites based on $M_3(HT)_1$ organoclay show the most significant improvement in organoclay exfoliation.

From the above, it is clear that adding the polar vinyl acetate groups to the polymer matrix improves the level of exfoliation achieved evidently due to an improved interaction between the organoclay and the polymer. Within the range of VA contents examined, nanocomposites formed from the $M_2(HT)_2$ organoclay have the best exfoliation compared with the other two organoclays; however, the differences in exfoliation among the different organoclays become smaller as the VA content of the polymer matrix is increased.

3.1.2. Particle analysis

To have a quantitative assessment of the relationship between the level of organoclay exfoliation and nanocomposite properties, detailed particle analyses were conducted on the TEM images using the method described earlier. For the best statistical reliability, a large number of particles (>300) should be analyzed for each nanocomposite. But this criterion could not be completely fulfilled in cases of poor exfoliation like LDPE/$M_3(HT)_1$ nanocomposites, where each image contains only one or two large agglomerates. The statistical results of particle analysis on nanocomposites containing 5 wt% MMT are listed in Table 3. The average particle lengths for all these nanocomposites are larger than those observed for nylon 6 nanocomposites, where nearly all the particles are individual platelets, i.e., essentially ideal exfoliation. We believe that the primary reason for the larger particles seen here is due to "skewing" of the platelets in these thicker clay bundles, as described by Chavarria and Paul [23]; however, some attrition of platelets during compounding may be possible. We also note that the aspect ratios calculated by averaging the values for each particle, $\langle l/t\rangle_n$ and $\langle l/t\rangle_w$, are always larger than those calculated from the ratio of the corresponding average particle length and average particle thickness, i.e., $\bar{l}_n/\bar{t}_n$ and $\bar{l}_w/\bar{t}_w$. The ratio of number average particle length and thickness ($\bar{l}_n/\bar{t}_n$) is generally larger than the ratio of the weight average particle length and thickness ($\bar{l}_w/\bar{t}_w$); however, the weight average aspect ratio calculated from the values for individual particles, $\langle l/t\rangle_w$, is always larger than the corresponding number average ratio, $\langle l/t\rangle_n$, as expected.

Fig. 3 shows a series of representative histograms of particle length, thickness and aspect ratio for EVA-28 based nanocomposites containing ~5 wt% MMT. All of the features, i.e., particle length, thickness and aspect ratio, showed broad distributions based on the analysis of a total of 611 particles.

To get a better idea of the relationship between the polarity of the polymer matrix, as defined by VA content, and the interaction with the organoclay, number average particle lengths and thicknesses of nanocomposites containing ~5 wt% MMT are presented in Fig. 4(a) and (b) as a function of vinyl acetate content in the polymer matrix. Similar plots for two types of average particle aspect ratios are shown in Fig. 4(c) and (d). As it turns out, the values of $\langle l/t\rangle_n$ are significantly higher than the corresponding values of ($\bar{l}_n/\bar{t}_n$) in all cases. For each series of nanocomposites prepared from a given organoclay, both the average particle length and the thickness decrease with increased VA content, but the aspect ratio using either method of averaging increases with VA content. The nanocomposites formed from the $M_2(HT)_2$ organoclay usually have the smallest particle length and thickness but the highest aspect ratio; but the differences in size and aspect ratio among nanocomposites formed from the various organoclays become smaller as the VA content increases and are almost unnoticeable at 40% VA.

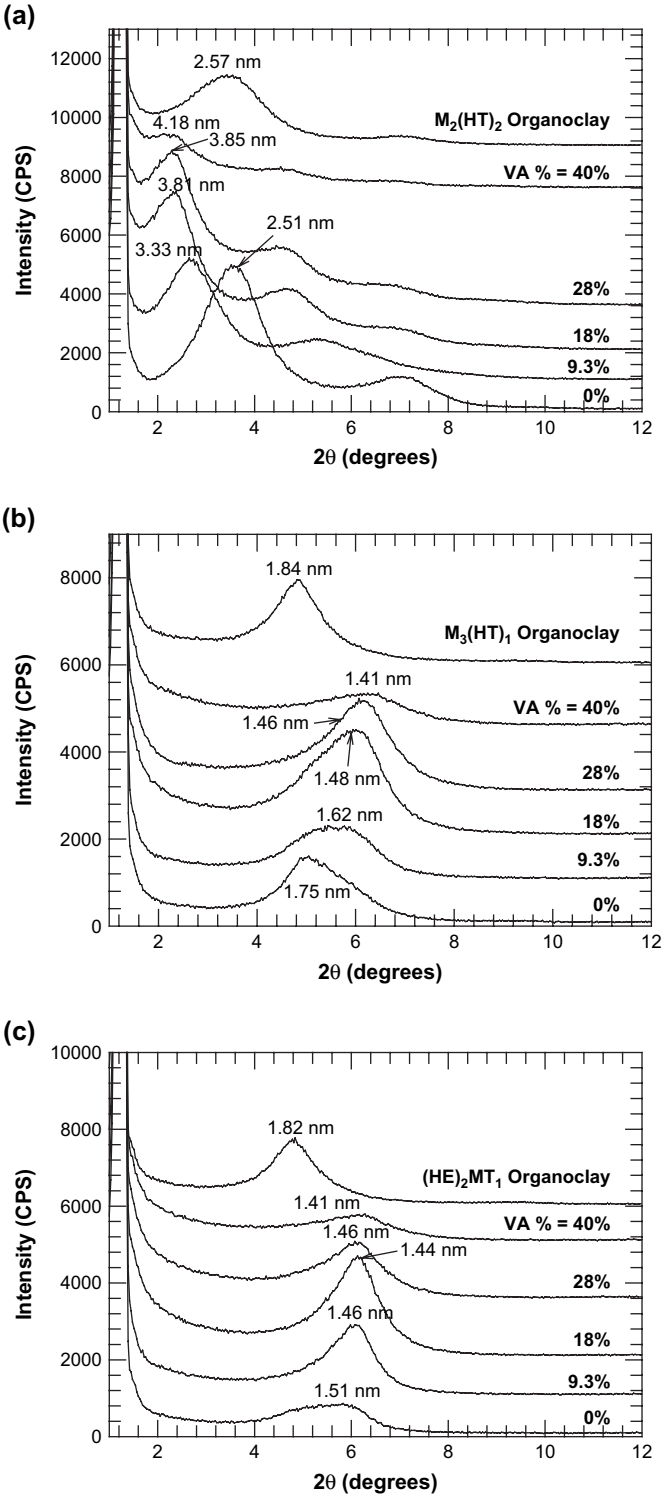

Fig. 5. WAXS scans for (a) $M_2(HT)_2$, (b) $M_3(HT)_1$, and (c) $(HE)_2M_1T_1$ pristine organoclays and nanocomposites containing ~5 wt% MMT formed from EVA copolymers with various VA contents. The curves are vertically offset for clarity.

3.1.3. WAXS

Wide angle X-ray scattering is another commonly used method to characterize the clay exfoliation in nanocomposites. WAXS scans of nanocomposites containing ~5 wt% MMT prepared from various polymer matrices and organoclays are presented in Fig. 5; scans for the neat organoclays are also included for comparison. All the nanocomposites, regardless of VA content or organoclay, show a distinct peak indicative of

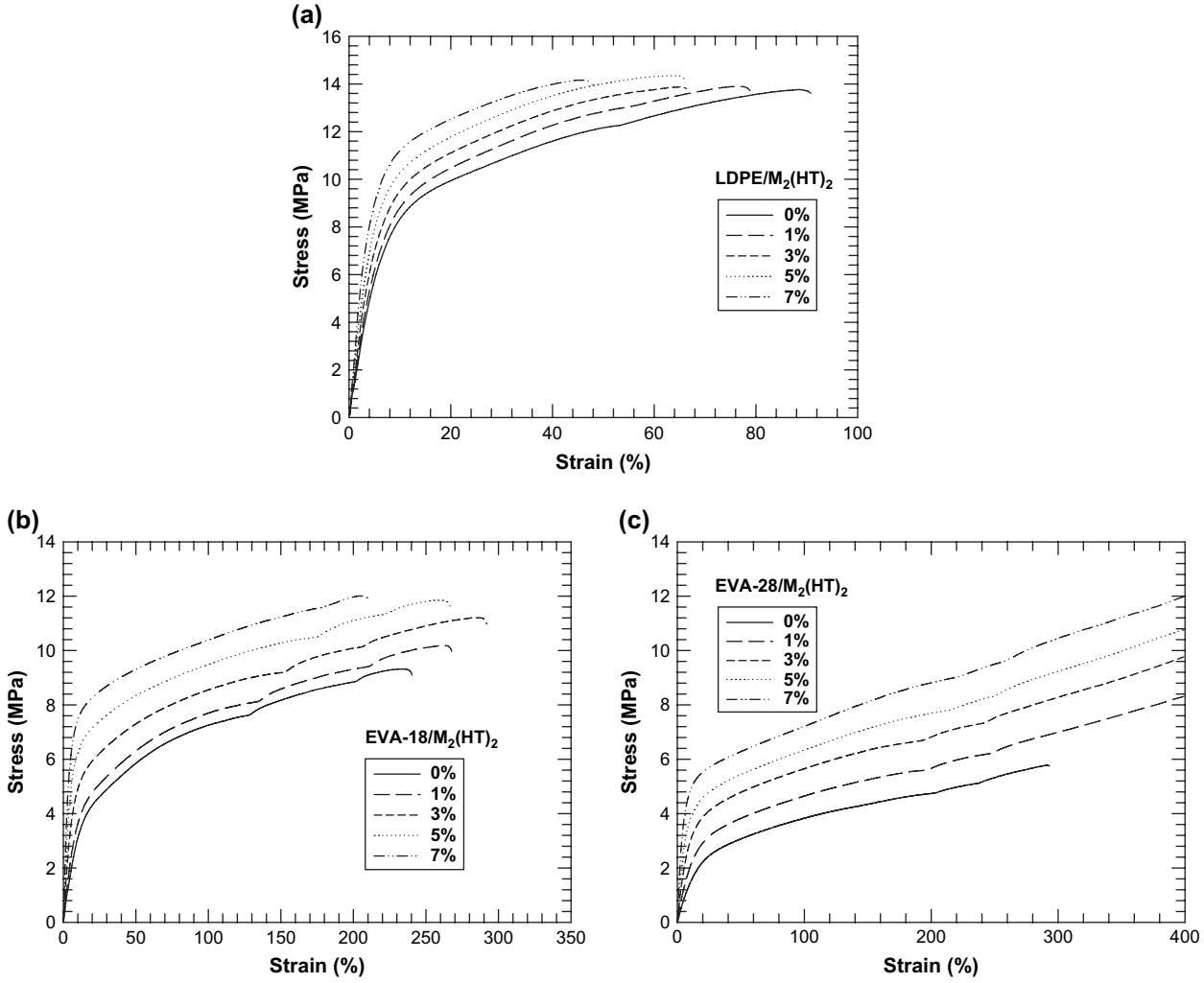

Fig. 6. Stress–strain diagrams for nanocomposites based on the $M_2(HT)_2$ organoclay and various EVA copolymers (a) LDPE, (b) EVA-18, and (c) EVA-28. The crosshead speed was fixed at 5.1 cm/min.

the presence of unexfoliated tactoids at positions shifted with respect to the peak of the pristine organoclay.

The scans for nanocomposites formed from the $M_2(HT)_2$ organoclay are shown in Fig. 5(a). For composites based on LDPE, the d_{001} peak remains at about the same position as that for the neat organoclay. For EVA based nanocomposites, the d_{001} peak shifts to the left more progressively the higher the VA level, and the peak intensity decreases with increasing VA content. This can be explained by the hypothesis that intercalation is a precursor to exfoliation [9,24]. According to prevalent proposals in the literature, shifting of the d_{001} peak to the left, i.e., lower angles, indicates an expanded d-spacing caused by intercalation of polymer or low-molecular weight oligomers in the gallery of the clay platelets and suggests a more intercalated/exfoliated structure.

For nanocomposites prepared from the $M_3(HT)_1$ and $(HE)_2M_1T_1$ organoclays, see Fig. 5(b) and (c), the WAXS results show a more complex and somewhat confusing picture. The d_{001} peak is progressively shifted to the right as the VA content of the polymer matrix increases, which is just the opposite of what might be expected based on the notion of intercalation being a precursor of exfoliation since TEM shows that exfoliation increases with VA content [9,24]. Similar peak shifts to lower d-spacings have been reported for LLDPE [9], LDPE [24], polystyrene [25], and poly(ethylene-*co*-methacrylic acid) [8] ionomer based nanocomposites especially when formed from one-tailed organoclays. Shah et al. attributed this to the degradation of the surfactant, which causes the clay galleries to collapse as surfactant mass is lost from within the galleries [8]. The fact that shifts to lower d-spacing are significant only for the one-tailed organoclays is consistent with degradation of the organic modifier during processing since they have been shown to be less thermally stable than the organoclays with multiple tails [9]. However, in the present case, the EVA nanocomposites were processed at 170 °C which is a relatively low temperature where surfactant degradation is not expected to be severe. Furthermore, the continuous shift to lower d-spacing with increasing VA content is also difficult to explain unless, of course, there is some chemical process by which the presence of VA units contributes to surfactant degradation. Clearly, a more detailed study will be needed to understand these observations.

3.2. Mechanical properties

The extent to which addition of organoclay to a polymer matrix alters mechanical properties provides another way to judge the extent of organoclay exfoliation in the polymer matrix.

3.2.1. Stress–strain behavior

Fig. 6 shows representative stress–strain curves for the nanocomposites prepared from the $M_2(HT)_2$ organoclay and EVA matrices with various VA contents. The stress–strain diagrams reveal no distinct yield point for either the neat polymer or the nanocomposites. As expected, the stress at any given strain level is increased as the content of MMT increases. As the VA content of the neat EVA materials increases, crystallinity decreases, causing the modulus to decrease and the elongation at break to increase; indeed, the elongation at break increases from below 100% for LDPE to more than 400%, the upper limit of crosshead travel of the instrument used here, for some materials with high VA content.

Fig. 7 shows that the stress at 40% strain is highest in samples made from $M_2(HT)_2$ organoclay, while the $M_3(HT)_1$ and the $(HE)_2M_1T_1$ organoclays show lower stresses for each series of nanocomposites based on the same matrix. As the MMT content increases, the stress at 40% strain increases significantly except for the nanocomposites formed from $M_2(HT)_2$ or $(HE)_2M_1T_1$ organoclay and LDPE or EVA-9.3, where the organoclay is poorly dispersed.

The effect of organoclay structure and VA content of the polymer matrix on elongation at break could not be fully evaluated since some samples (nanocomposites based on EVA-28) did not break before the Instron machine limit of 400% elongation. Fig. 8 compares the elongation at break for nanocomposites made from the three organoclays and LDPE, EVA-9.3, or EVA-18. Generally, as the clay content is increased, ductility decreases for nanocomposites based on LDPE and EVA-9.3. For EVA-18 based nanocomposites the trends are not so simple as may be seen in Fig. 8(c). For nanocomposites formed from the $M_2(HT)_2$ organoclay, the elongation at break first increases with MMT loading, reaches a maximum at 3 wt% MMT and then decreases as more MMT is added. For nanocomposites formed from the $(HE)_2M_1T_1$ organoclay, elongation at break is relatively unaffected by the MMT content, while all the nanocomposites formed from the $M_3(HT)_1$ organoclay have slightly higher elongations at break than the neat polymer.

3.2.2. Modulus

Fig. 9 compares the tensile moduli of the nanocomposites formed from different organoclays, based on the same matrix, as a function of their montmorillonite content. As expected, the stiffness improves with addition of organoclay; however, the increase is always much stronger for the organoclay with two alkyl tails, $M_2(HT)_2$, than for the others with one alkyl tail, i.e., $M_3(HT)_1$ and $(HE)_2M_1T_1$. This supports the TEM observations that the nanocomposites formed from the $M_2(HT)_2$ organoclay have better exfoliation than those formed from the other organoclays.

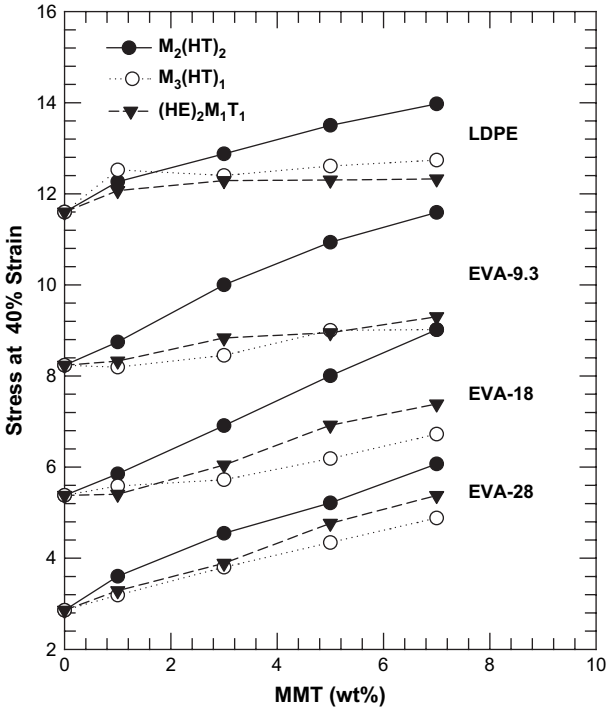

Fig. 7. Stress at a strain of 40% for nanocomposites formed from various EVA copolymers and organoclays.

Since the moduli of the neat EVA polymers vary in a great deal with VA content owing to changes in crystallinity, it is useful to examine the relative moduli of the nanocomposites versus the montmorillonite content as shown in Fig. 10. For nanocomposites formed from the $M_3(HT)_1$ organoclay, the relative modulus at a given MMT content increases continuously as the VA content of the polymer matrix is increased, suggesting better exfoliation with an increased amount of the polar component in the matrix, as shown by TEM. In contrast, for nanocomposites formed from $M_2(HT)_2$ and $(HE)_2M_1T_1$, the relative modulus at a given MMT content increases as the VA content increases up to about 18%, but a further increase to 28% leads to a slightly lower relative modulus. In this regard, the moduli data are not in complete accord with the TEM particle analysis, which revealed improvements in exfoliation with increased VA content over the entire range (0–40% VA) examined. Inconsistencies between relative moduli and TEM morphologies have been suggested in previous work from this laboratory [9,26]. Further work will explore the sources of such inconsistencies. One possible explanation may be that the matrix properties are altered, e.g., by changes in crystallinity and by the presence of the nanoscale clay particles.

3.3. Composite model predictions of modulus

Theoretical modeling is an appealing approach for the design of polymer nanocomposite systems, and numerous

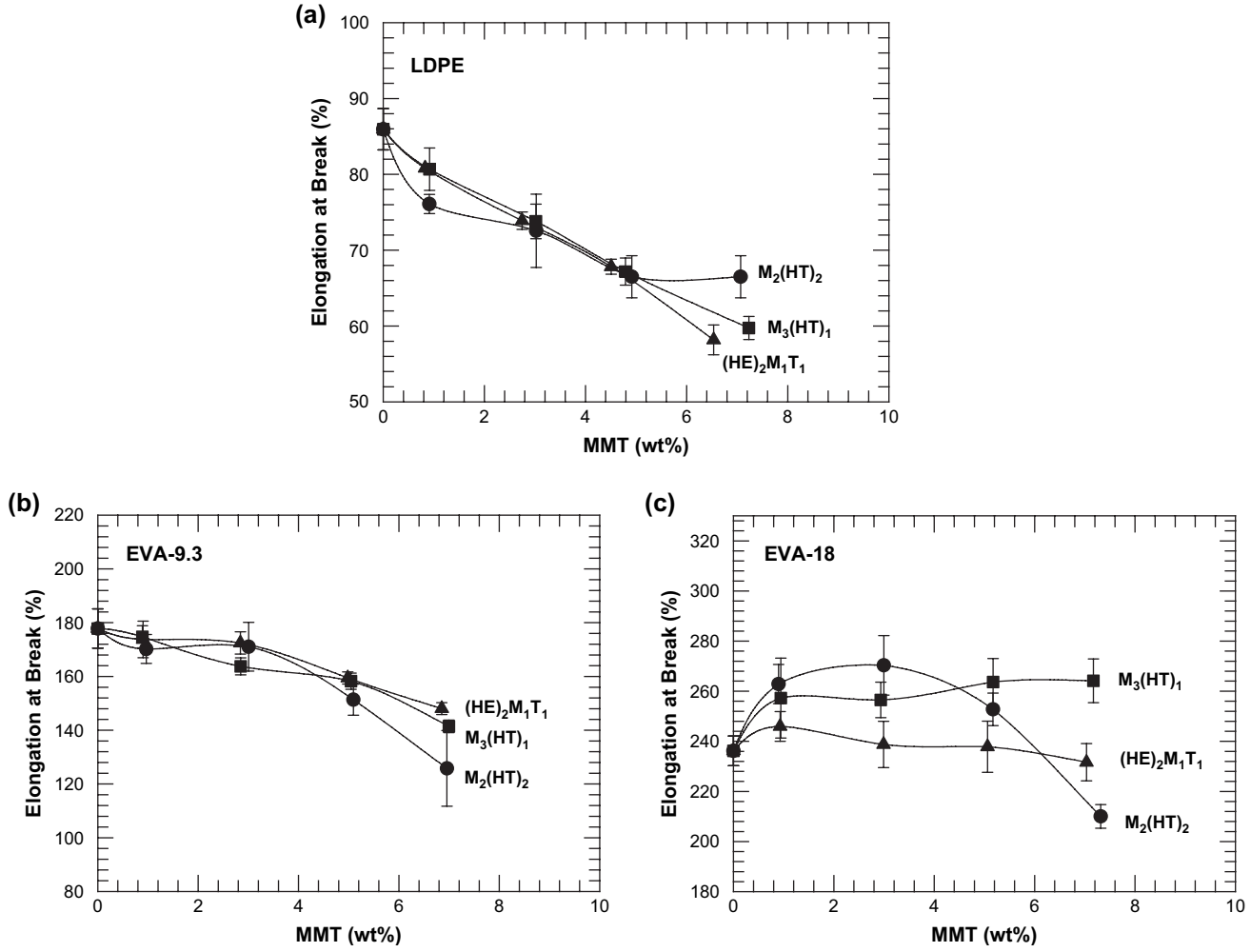

Fig. 8. Elongation at break for nanocomposites formed from various organoclays and EVA copolymers (a) LDPE, (b) EVA-9.3, and (c) EVA-18.

models [27–30] have been proposed to predict the properties of nanocomposites or for correlation of experimental data. However, there are numerous assumptions implicit within the use of such models that must be kept in mind. For example, it is assumed that the polymer matrix is not affected by the presence of the filler, the filler is perfectly aligned, the matrix and the filler are isotropic, and there are no particle–particle interactions or agglomerations [31].

Halpin–Tsai and Mori–Tanaka models are widely used to predict the tensile modulus of composites. Halpin–Tsai equations treat the fillers as rectangular platelets of constant thickness, whereas Mori–Tanaka theory considers them as ellipsoidal particles and takes account of the Poisson ratios of the filler and the matrix. Previous work in this laboratory and others [23,26,31,32] has shown that both theories predict similar trends for the tensile modulus, but Mori–Tanaka theory tends to give lower estimates of modulus than Halpin–Tsai equations [16,23,32] at low filler loadings. A more detailed discussion on the similarities and differences between these two models has been given by Fornes and Paul [31].

For simplicity, Halpin–Tsai equations were employed in this work to relate the longitudinal tensile modulus of nanocomposites prepared in this study to the nanocomposite morphology determined by TEM. The predicted modulus depends on the volume fraction of the filler ϕ_f, the filler/matrix modulus ratio E_p/E_m, the filler aspect ratio l/t [33,34], and filler orientation. The expression for the longitudinal modulus [26,31,32] is:

$$\frac{E^{(H-T)}}{E_m} = \frac{1 + 2(l/t)\phi_f \eta}{1 - \phi_f \eta} \tag{1}$$

where η is given by

$$\eta = \frac{(E_p/E_m) - 1}{(E_p/E_m) + 2(l/t)} \tag{2}$$

In these model calculations, the partially exfoliated clay particles were treated as parallel arrangements of MMT platelets and gallery material as described in previous reports [26,31,32,35]. The tensile modulus of such an effective particle can be estimated by using the following rule of mixtures:

$$E_p = \nu_{MMT} \times E_{MMT} + \nu_{gallery} \times E_{gallery} \tag{3}$$

where ν_{MMT} and $\nu_{gallery}$ are the volume fraction of montmorillonite and gallery space in the effective particle, while E_{MMT}

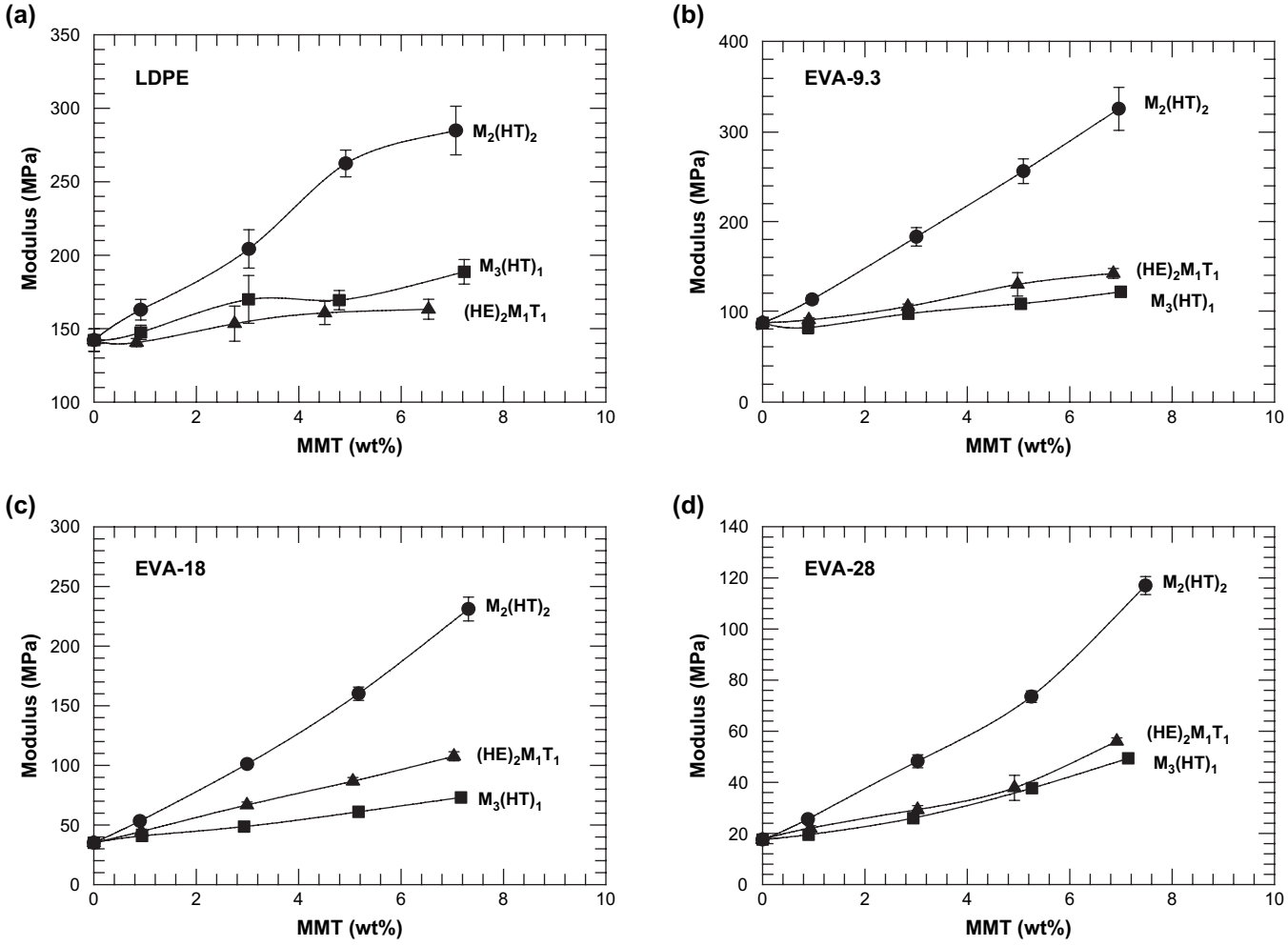

Fig. 9. Modulus as a function of montmorillonite content of nanocomposites formed from various organoclays and EVA copolymers (a) LDPE, (b) EVA-9.3, (c) EVA-18, and (d) EVA-28.

and E_{gallery} are their corresponding moduli. The volume fraction of MMT platelets, v_{MMT}, is calculated as the ratio of the thickness of an individual platelet and the d-spacing of the nanocomposite as determined by the WAXS analysis:

$$v_{\text{MMT}} = \frac{t_{\text{platelet}}}{d_{001}} \tag{4}$$

Considering that the modulus of the organic material in the gallery is significantly smaller than the modulus of the MMT platelets, Eq. (3) reduces to

$$E_{\text{p}} = v_{\text{MMT}} \times E_{\text{MMT}} \tag{5}$$

A WAXS scan of EVA-9.3/$M_2(HT)_2$ nanocomposite containing ~5 wt% MMT shows a d-spacing of 3.33 nm, so v_{MMT} is estimated to be $v_{\text{MMT}} = t_{\text{platelet}}/d_{001} = 0.94\ \text{nm}/3.33\ \text{nm} = 0.282$, where 0.94 nm is the thickness of an individual MMT platelet. Taking 178 GPa as the modulus of montmorillonite platelets and $v_{\text{MMT}} = 0.282$ in Eq. (5), we estimate the modulus of the effective modulus of an incompletely exfoliated MMT particle as $E_p = v_{\text{MMT}} \times E_{\text{MMT}} = 178\ \text{GPa} \times 0.282 = 50.2\ \text{GPa}$. The other parameters involved in the model calculations for nanocomposites containing ~5 wt% MMT are listed in Table 4.

Fig. 11(a) and (b) compares the experimental tensile moduli of nanocomposites with that predicted by Halpin–Tsai equations. The modulus of the nanocomposites containing ~5 wt% MMT generally decreases as VA content increases owing to the large decrease in E_{m}, but the relative modulus goes up due to the increase of the aspect ratio. In Fig. 11(c) and (d), the experimental relative tensile modulus of the nanocomposites and predictions by Halpin–Tsai equations are compared. Number average aspect ratios from the particle analysis described earlier defined as $\langle l/t \rangle_{\text{n}}$ and $(\bar{l}_{\text{n}}/\bar{t}_{\text{n}})$ were both used to make the model predictions. The model predictions show a reasonable parallel with the experimental data regardless of which average aspect ratio is used; however, the agreement between model and experiment is somewhat better when the $\bar{l}_{\text{n}}/\bar{t}_{\text{n}}$ measure of aspect ratio is used.

4. Conclusions

Nanocomposites based on a series of EVA copolymers containing 0–40% VA and three organoclays, $M_2(HT)_2$, $M_3(HT)_1$ and $(HE)_2M_1T_1$, were made to explore how the affinity between the organoclay and EVA copolymers changes with VA content. The degree of exfoliation of the nanocomposites

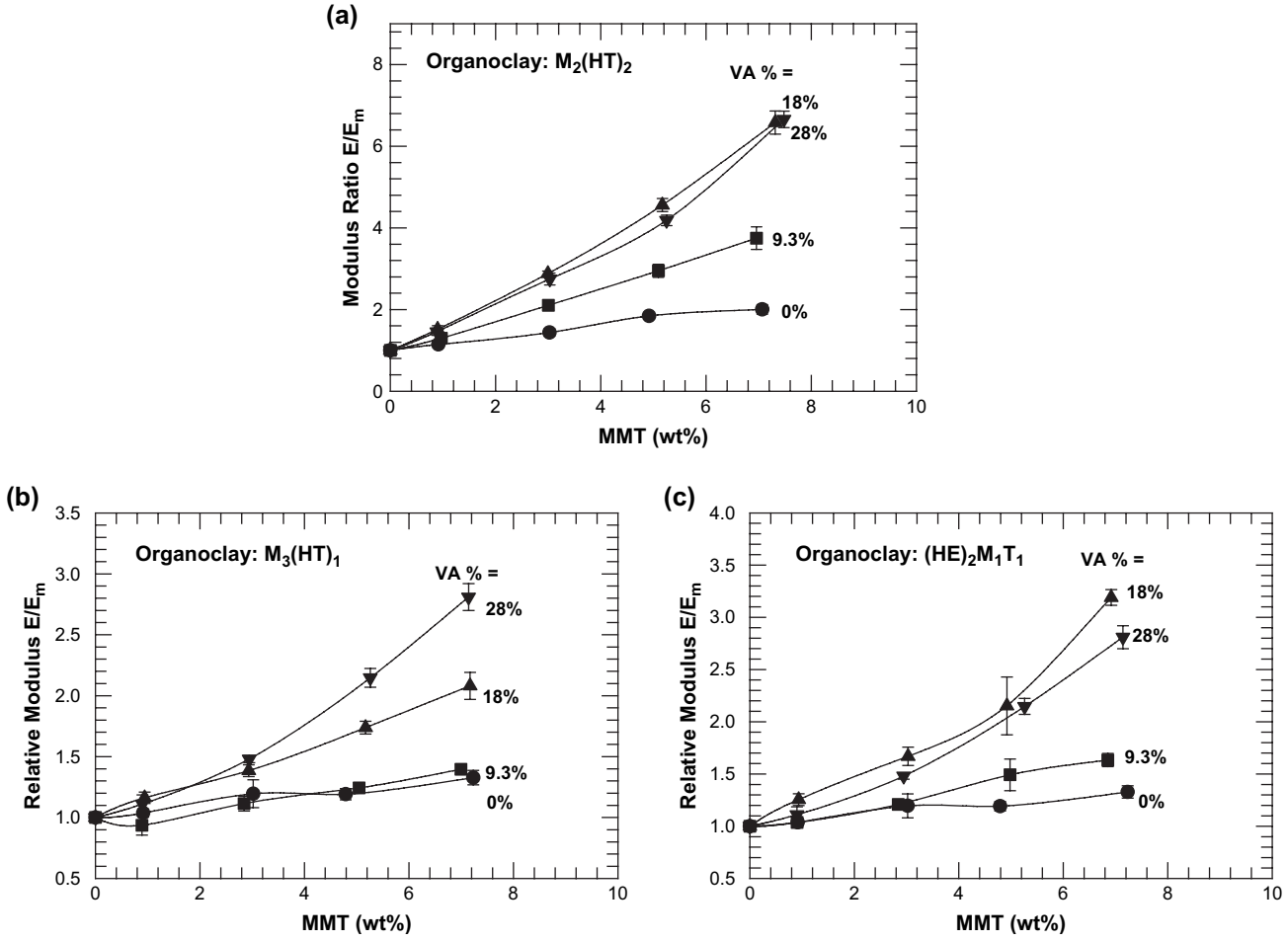

Fig. 10. Relative modulus as a function of montmorillonite content of nanocomposites formed from various EVA copolymers and organoclays (a) $M_2(HT)_2$, (b) $M_3(HT)_1$, and (c) $(HE)_2M_1T_1$.

was evaluated by TEM, WAXS, and mechanical testing. Broadly speaking, the results from the different techniques are consistent with each other.

As reported previously, the organoclay based on the surfactant with two alkyl tails, $M_2(HT)_2$, gives the best exfoliation in low density polyethylene, LDPE. The organoclay based on surfactant with a single alkyl tail, $M_3(HT)_1$, leads to slightly better exfoliation than the one containing hydroxy-ethyl groups, $(HE)_2M_1T_1$. As the vinyl acetate content of the EVA copolymers is increased, the degree of exfoliation for all these

Table 4
Parameters used in Halpin–Tsai Model[a]

Polymer matrix	Organoclay	*d*-Spacing (d_{001}, nm)	Vol. fraction of MMT in particle (ν_{MMT})	Modulus of particle (E_p, GPa)	Modulus of the polymer matrix (E_m, MPa)	Weight fraction of MMT in nanocomposites (%)	Vol. fraction of the filler in nanocomposites (ϕ_f)
LDPE	$M_2(HT)_2$	2.51	0.375	66.7	142.2	4.92	0.0427
EVA-9.3		3.33	0.282	50.2	86.9	5.09	0.0589
EVA-18		3.81	0.247	43.9	35.1	5.17	0.0688
EVA-28		3.85	0.244	43.5	17.6	5.25	0.0702
LDPE	$M_3(HT)_1$	1.75	0.537	95.6	142.2	4.79	0.0295
EVA-9.3		1.62	0.580	103.3	86.9	5.05	0.0289
EVA-18		1.48	0.635	113.0	35.1	5.17	0.0272
EVA-28		1.46	0.644	114.6	17.6	5.26	0.0284
LDPE	$(HE)_2M_1T_1$	1.51	0.623	110.8	142.2	4.51	0.0240
EVA-9.3		1.46	0.644	114.6	86.9	4.98	0.0262
EVA-18		1.44	0.653	116.2	35.1	5.06	0.0266
EVA-28		1.46	0.644	114.6	17.6	4.92	0.0262

[a] Nanocomposites contain nominally 5 wt% MMT, and all the nanocomposites here were modeled as partially exfoliated composites.

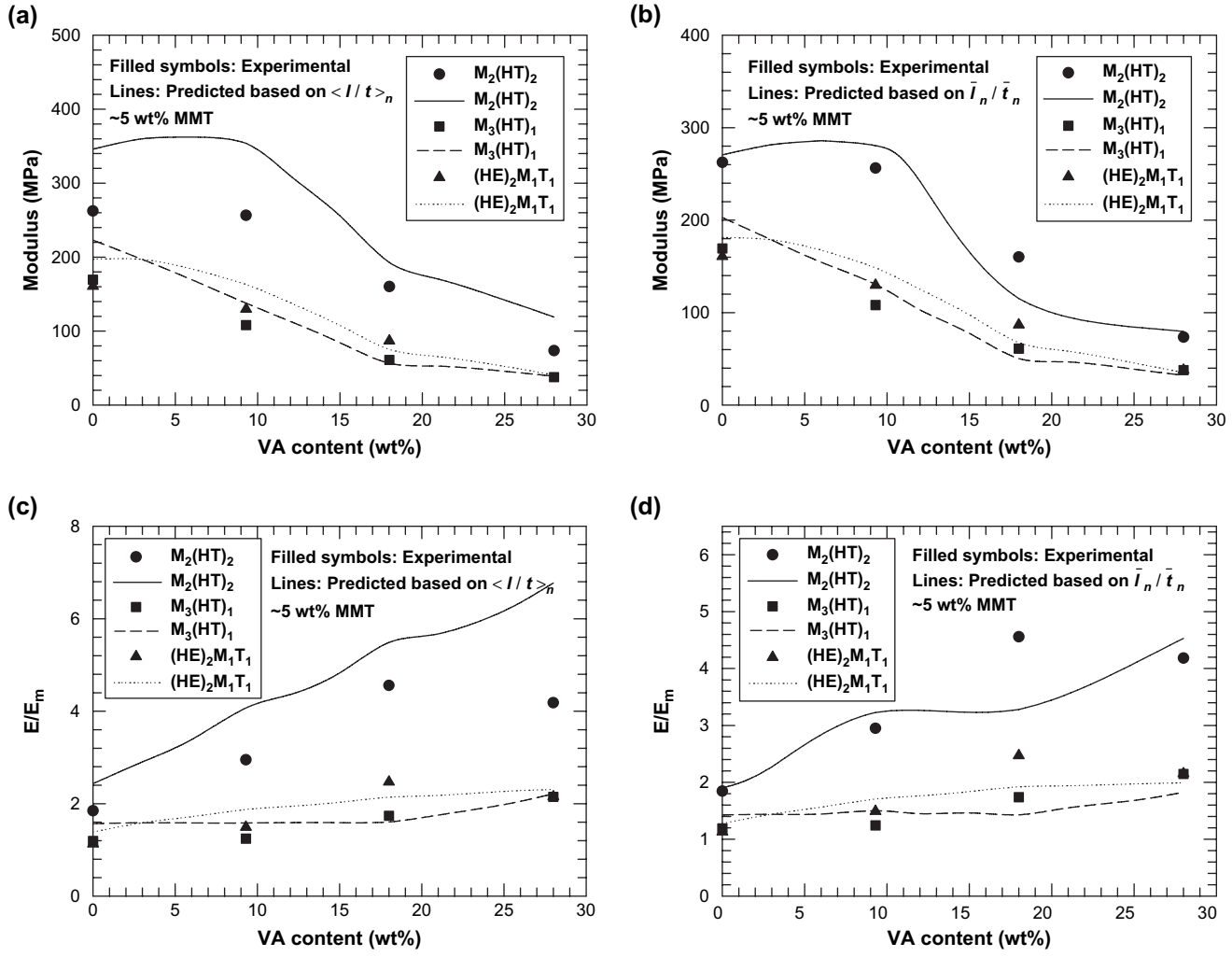

Fig. 11. Comparison of experimental tensile modulus and relative modulus of nanocomposites with predictions by Halpin–Tsai Model.

organoclays is dramatically increased. Up to 40 wt% VA, the organoclay with two alkyl tails always gives better exfoliation than either organoclay with a single tail. However, the relative advantage of the two tails versus one tail seems to diminish with increased VA level, but the advantage is never reversed indicating that even at 40 wt% VA, EVA copolymers interact with the organoclay more similar to polyolefins than polyamides which give better exfoliation with organoclays based on surfactants with a single tail. As the VA content increases, the relative advantage of $M_3(HT)_1$ versus $(HE)_2M_1T_1$ seems to reverse but the effect is not large. The hydroxyl groups on the $(HE)_2M_1T_1$ organoclay may interact with the EVA polar groups or the silicate surface, and this competition may account for some of this behavior.

The morphology of the nanocomposites formed from these organoclays and the various EVA copolymer matrices was quantified by analysis of TEM images to give various averages of the clay particle dimensions and shape. In all cases, the particles become smaller as the VA content of the matrix increases since the more favorable interaction with the matrix leads to better break down of the clay particle aggregates; however, the aspect ratio of the particles increases as the VA content increases. A simple composite model based on Halpin–Tsai equations was used to show that there is rather good quantitative agreement between the predicted values of modulus calculated from the TEM results and that measured experimentally.

Acknowledgements

The authors thank D. L. Hunter of Southern Clay Products, Inc. for many helpful discussions and for providing materials and other assistance.

References

[1] Okada A, Fukushima Y, Kawasumi M, Inagaki S, Usuk A, Sugiyami S, et al. US Patent No. 4739007; 1988 [assigned to Toyota Motor Co., Japan].
[2] Reichert P, Nitz H, Klinke S, Brancsch R, Thomann R, Mulhaupt R. Macromolecular Materials and Engineering 2000;275:8–17.
[3] Dennis HR, Hunter DL, Chang D, Kim S, White JL, Cho JW, et al. Polymer 2001;42(23):9513–22.
[4] Fornes TD, Yoon PJ, Hunter DL, Keskkula H, Paul DR. Polymer 2002;43(22):5915–33.
[5] Fornes TD, Hunter DL, Paul DR. Macromolecules 2004;37(5):1793–8.

[6] Kim DH, Fasulo PD, Rodgers WR, Paul DR. Annual Technical Conference—Society of Plastics Engineers 2006;64:592–6.
[7] Lee H-s, Fasulo PD, Rodgers WR, Paul DR. Polymer 2005; 46(25):11673–89.
[8] Shah RK, Hunter DL, Paul DR. Polymer 2005;46(8):2646–62.
[9] Hotta S, Paul DR. Polymer 2004;45(22):7639–54.
[10] Beyer G. Fire and Materials 2002;25(5):193–7.
[11] Jang BN, Costache M, Wilkie CA. Polymer 2005;46(24):10678–87.
[12] Gao F, Beyer G, Yuan Q. Polymer Degradation and Stability 2005;89(3):559–64.
[13] Zanetti M, Camino G, Mulhaupt R. Polymer Degradation and Stability 2001;74(3):413–7.
[14] Zanetti M, Camino G, Thomann R, Mulhaupt R. Polymer 2001;42(10): 4501–7.
[15] Fornes TD, Yoon PJ, Keskkula H, Paul DR. Polymer 2001;42(25): 09929–40.
[16] Stretz HA, Paul DR, Li R, Keskkula H, Cassidy PE. Polymer 2005;46(8):2621–37.
[17] Stretz HA, Paul DR. Polymer 2006;47(26):8527–35.
[18] Paul DR, Zeng QH, Yu AB, Lu GQ. Journal of Colloid and Interface Science 2005;292(2):462–8.
[19] Paul DR. Abstracts of papers, 229th ACS national meeting. San Diego, CA, United States; 13–17 March, 2005. 2005POLY-205.
[20] Shah RK, Krishnaswamy RK, Paul DR. Annual Technical Conference—Society of Plastics Engineers 2006;597–601.
[21] Shah RK, Paul DR. Macromolecules 2006;39(9):3327–36.
[22] Chavarria F, Paul DR. Polymer 2006;47(22):7760–73.
[23] Chavarria F, Paul DR. Polymer 2004;45(25):8501–15.
[24] Shah RK, Paul DR. Polymer 2006;47(11):4075–84.
[25] Tanoue S, Utracki LA, Garcia-Rejon A, Tatibouet J, Cole KC, Kamal MR. Polymer Engineering and Science 2004;44(6):1046–60.
[26] Shah RK, Kim DH, Paul DR. Polymer 2007;48(4):1047–57.
[27] Hill R. Journal of the Mechanics and Physics of Solids 1965;13(4): 213–22.
[28] Hill R. Proceedings of the Physical Society London 1952;65(A):349–54.
[29] Halpin JC. Journal of Composite Materials 1969;3(4):732–4.
[30] Halpin JC, Affdl JLK. Polymer Engineering and Science 1976;16(5): 344–52.
[31] Fornes TD, Paul DR. Polymer 2003;44(17):4993–5013.
[32] Sheng N, Boyce MC, Parks DM, Rutledge GC, Abes JI, Cohen RE. Polymer 2004;45(2):487–506.
[33] Ashton JF, Halpin JC, Petit PH. Primer composite materials analysis. USA: Technomic; 1969.
[34] Chow TS. Journal of Polymer Science: Polymer Physics Edition 1978;16(6):959–65.
[35] Brune DA, Bicerano J. Polymer 2002;43(2):369–87.